Artemis: Surface expression of a deep mantle plume on Venus

Vicki L. Hansen*
Department of Geological Sciences, Southern Methodist University, Dallas, Texas 75275, USA

ABSTRACT

Artemis, a unique 2600-km-diameter circular feature on Venus, defies geomorphic classification as a corona, crustal plateau, or volcanic rise. Artemis is similar in size to plateaus and rises, yet topographically resembles a corona. Geologic mapping using correlated digital remote data sets including NASA *Magellan* C1-, C2-, and F-scale synthetic aperture radar (SAR) imagery, altimetry, and synthetic stereo has led to a determination of the geologic history of Artemis. Artemis comprises a large topographic welt that includes a paired circular ~1-km-deep trough (Artemis Chasma) and ~1-km-high outer rise; thus, Artemis is divisible into chasma (trough), interior region, and exterior region. The chasma hosts trough-normal faults and folds. The interior includes five ~350-km-diameter coronae (quasi-circular features marked by radial and/or concentric fractures) that record rich tectono-volcanic histories; radial extension fractures and trough-concentric wrinkle ridges dominate the exterior tectonic fabric. Artemis formed as a coherent entity; the coronae, chasma, chasma structures, radial fractures, and wrinkle ridges are all consistent with a deep plume model for Artemis formation. Rising and flattening of the plume head led to early uplift, doming, and radial fracturing as the plume head collapsed vertically and spread laterally, likely causing outward migration of the trough, as well as fracturing and wrinkle-ridge formation outboard of the trough. Within the trough, material was pulled downward, forming normal faults and folds. The plume continued to spread laterally outboard of the trough, resulting in continued radial fracturing and wrinkle-ridge formation. Small-scale interior convection cells or compositional diapirs resulted in coronae with radial fractures, and/or concentric fractures and/or folds, and associated volcanism. Artemis is akin in its formation to crustal plateaus and volcanic rises and likely formed during the transition from globally thin to thick lithosphere.

Keywords: coronae, diapirs, plateaus, plumes, synthetic aperture radar (SAR), Venus.

INTRODUCTION

Understanding Artemis, a unique 2600-km-diameter circular feature located in Venus's Southern Hemisphere, represents a challenging puzzle in the tectonics of Venus because Artemis differs from all other features on Earth's sister planet. Artemis's planform shape and size resemble quasi-circular crustal plateaus and volcanic rises (diameter ranges of ~1600–2500 km), but differ from these features topographically. Crustal plateaus display steep-sided flat-topped regions, and volcanic rises describe broad domical forms, whereas Artemis is defined by a 1–2-km-deep, ~2100-km-diameter circular trough (chasma) that encompasses a moderately high interior. By contrast, coronae—small- to moderate-sized circular to quasi-circular features that display radial to concentric fractures or faults and variable evidence of volcanism—commonly host circular troughs that are topographically similar to Artemis Chasma. However, Artemis is approximately twice the size of the largest corona, Hengo Corona (1060 km diameter) and more than an order of magnitude larger than median coronae (200 km diameter). In addition, Artemis's interior is structurally quite different from that of coronae. Artemis is not obviously classified as a volcanic rise, crustal plateau, or corona (Hansen et al., 1997; Stofan et al., 1997). Thus, Artemis defies classification as, or correlation with, other geomorphic features on Venus.

With the exception of Artemis, all of Venus's major geomorphic features can be accommodated in a model in which the Venusian lithosphere increased in thickness over time (Phillips and Hansen, 1998). Crustal plateaus and volcanic rises represent the surface signatures of deep mantle plumes on ancient thin and contemporary thick lithosphere, respectively. Widespread plains volcanism resulted from pressure-release melting during the thin-lithosphere time, whereas large topographic basins on the plains record contemporary broad convective downwellings (Herrick and Phillips, 1992; Rosenblatt and Pinet, 1994; Sandwell et al., 1997). Ishtar Terra formed during the thin-lithosphere time and represents a crustal plateau welt (expressed at Fortuna Tessera) and other crust captured within an ancient broad convective downwelling and preserved by mantle-melt residuum at depth (Hansen and Phillips, 1995; Hansen et al., 1997). Coronae represent surface expressions of mantle diapirs (e.g., Squyres et al., 1992; Stofan et al., 1992, 1997) probably formed during both thin- and thick-lithosphere time. Many coronae contribute to relatively recent volcanic resurfacing in some plains basins (Guest and Stofan, 1999; Young et al., 2000; Rosenberg and McGill, 2001; Hansen and DeShon, 2002, Hansen et al., 2002). Although some workers have suggested that Artemis represents a region of lithospheric underthrusting (Schubert et al., 1994; Brown and Grimm, 1995, 1996, 1999), such an interpretation is not easily reconciled with the local tectonic setting (Brown and Grimm, 1995), with the evolutionary picture just described or, as shown here, with Artemis's geologic relationships. Spencer (2001) interpreted a part of Artemis's interior as a region of extensive crustal extension similar to a terrestrial metamorphic core complex; he did not place the study within a regional or global context.

This paper examines the geology of Artemis and the surrounding region in order to determine the surface evolution of Artemis. In this paper, the term ''Artemis'' describes the large circular geomorphic feature centered at about 33°S, 133°E, including Artemis Chas-

*E-mail: vhansen@mail.smu.edu.

GSA Bulletin; July 2002; v. 114; no. 7; p. 839–848; 7 figures.

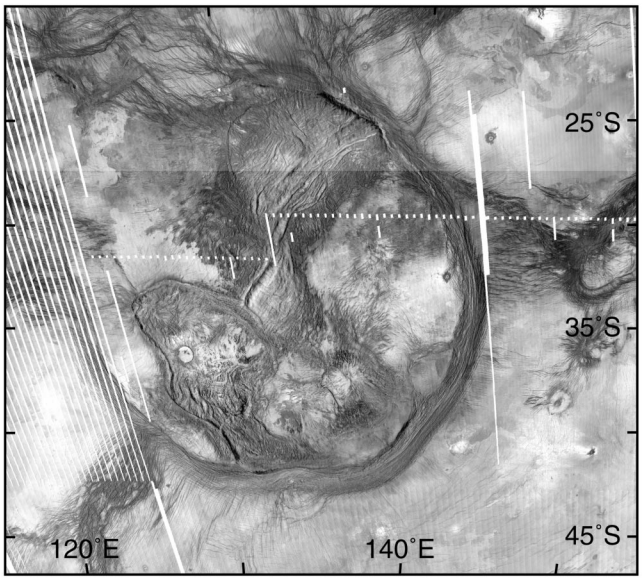

Figure 1. Negative SAR image of Artemis.

ma, the raised region interior to the chasma, and the adjacent exterior region (Fig. 1). This broad definition of Artemis frees one from assumptions of the spatial or temporal relationships of regions on either side of Artemis Chasma. The major tool of exploration used here is geologic mapping. The map shown herein is generally consistent with mapping of Brown and Grimm (1995), who had access to the same data, although the resulting interpretation differs from theirs. Artemis embodies three major features that collectively record deformation related to Artemis formation including Artemis Chasma and the regions interior and exterior to the chasma. Artemis hosts six coronae or corona-like features—five within its interior and one within the chasma. The data indicate that chasma, interior, and exterior all formed broadly contemporaneously and that together they record Artemis's evolution as the surface signature of a deep mantle plume; the coronae record either small-scale convection or compositional diapirs spawned from the hot thermal plume. Artemis's unique morphology, geologic character, and geologic history may indicate that Artemis formed during Venus's transition from thin to thick lithosphere.

DATA AND METHODOLOGY

The data resulted from the NASA *Magellan* Mission (1991–1994; Ford et al., 1993); correlated digital data sets used here include *Magellan* C1-, C2-, and F-scale synthetic aperture radar (SAR) imagery (~225, 675, and 110 m resolution, respectively), altimetry, and synthetic stereo imagery (Kirk et al., 1992). This analysis follows general Magellan data analysis and feature identification outlined by Ford et al. (1993) and mapping criteria described by Tanaka et al. (1994), with caveats highlighted by Hansen (2000). Structural-element and geologic-facies interpretations follow methods outlined previously (Keep and Hansen, 1994; Ghent and Hansen, 1999; Hansen et al., 2000). SAR images are either left-look (similar to left illumination) or right-look. As a general rule, radar brightness is a function of surface roughness and orientation; radar-bright regions are rough and/or oriented toward incident radar, whereas radar-dark regions are smooth or oriented away from radar (Ford et al., 1993); the opposite is true for negative SAR images shown herein. Structural facies typically show up better in negative images. Artemis's circular nature lends itself to an analogue clock reference frame with north at 12:00, east at 3:00, south at 6:00, and west at 9:00. Elevation on Venus is typically cited in relationship to mean planetary radius (MPR), 6051.84 km; this convention is followed herein.

This paper builds on the work of Brown and Grimm (1995) that focused on Artemis Chasma. Although Brown and Grimm (1995) used the same data set used here, my processing methods differ from theirs; Brown and Grimm (1995) used an airbrush shaded-relief approach to view three dimensions, whereas synthetic stereo images are used herein). Readers should refer to Brown and Grimm (1995) for regional overviews of Artemis topography and SAR imagery and for numerous detailed SAR and shaded-relief images that are extremely instructive in feature identification.

ARTEMIS GEOLOGY

The Venusian surface is dominantly composed of volcanic rocks; lack of surface water and the paucity of eolian erosion on Venus (e.g., Kaula, 1990) rules out major sedimentary packages, and the lack of widespread erosion makes exposure of crustal metamorphic or intrusive igneous rocks unlikely. Impact crater-related, landslide, or eolian deposits are present, but areally restricted. This analysis employs basic geologic- and structural-mapping methods in order to construct a geologic map of the Artemis's surface, aimed at understanding the nature of the spatial and temporal evolution of tectonism and volcanism across Artemis. Artemis consists of an ~2600-km-diameter topographic welt near the terminations of Diana and Dali chasmata (Fig. 1; Brown and Grimm, 1995, Figs. 1 and 2). The welt includes an ~2100-km-diameter, ~1-km-deep circular trough (Artemis Chasma) paired with an ~1-km-high outer rise (Sandwell and Schubert, 1992). Inward from the trough an inner rise reaches up to 4 km, but typical interior highs stand at 1.5–2 km; interior northeast- and northwest-trending high and lows are also preserved locally. A reduced version of the geologic map (Fig. 2) compiled at 1:5 000 000 scale agrees with the characterization and location of most structural features defined by Brown and Grimm (1995, Fig. 16); therefore, detailed justification of geologic-element identification is not discussed. The current map covers a slightly larger region and examines the interior geology in greater detail than that of Brown and Grimm (1995) and includes additional primary and secondary structures as well as additional geologic and radar units.

At Artemis, radar brightness is locally a function of both tectonic and volcanic fabrics that can be difficult to delineate at the scale of the data (e.g., Fig. 3A). A radar-bright facies is defined herein that includes Brown and Grimm's (1995) ''fine-scale fabric'' as a radar unit, but not as a geologic unit owing to its containing mixed genetic facies. The radar-bright facies occurs in the interior, exterior, and within the chasma (Fig. 2). Major trend(s) of penetratively developed tectonic fabrics (i.e., spaced at or below data resolution) marked by lineaments or suites of lineaments are highlighted. Where the character of the tectonic fabric is not clear, only the trends are represented. This radar facies does not repre-

sent a distinct geologic unit formed at a specific time; in both the interior and the exterior regions, the boundaries between radar-bright and -dark facies preserve a range of temporal relationships. Some flow units postdate tectonic patterns as evidenced by embayment relationships (e.g., Fig. 3A, C, and F), whereas in other cases, tectonism clearly postdates the radar-dark facies as evidenced by the feathering or jagged trace of tectonic fractures or faults (e.g. Fig. 3B and C). Earlier-formed tectonic fabrics are locally preserved as kipukas representing local highs protected by their elevation from low-viscosity lava flows (e.g., Fig. 3E and G). Examination of SAR and synthetic stereo imagery, discussed in detail in the following sections (Artemis Chasms, Interior Features, and Exterior Features), indicates that tectonism and volcanism were spatially and temporally intimately related throughout formation of the radar-bright and -dark facies and that the development of both the radar-bright and -dark facies was diachronous.

Artemis includes three major elements (Fig. 2): (1) Artemis Chasma, an almost complete (~300°) circular topographic trough that contains trough-parallel normal faults and folds; (2) an interior region that hosts five coronae (C1–C5) or corona-like features (e.g., Stofan et al., 1992)—variably defined by radial fractures (or faults), concentric fractures (or faults), and/or folds—that display contemporaneous volcanism and tectonism including numerous volcanic shields; and (3) an outboard region cut by trough-parallel wrinkle ridges and trough-normal fractures, the latter of which are locally overprinted by trough structures.

Artemis Chasma

Artemis Chasma lies 1–2 km below mean planet radius and ranges in width from ~25–150 km. The trough, which is well defined except from ~10:00 to 11:30, hosts a linear fabric that is penetratively developed at the scale of observation and that everywhere parallels the trough axis. The fabric consists of normal faults and folds as noted by Brown and Grimm (1995). Normal faults dominate the fabric from 11:30 to 2:00, whereas folds dominate from 6:00 to 10:30. Corona C6, defined by radial lineaments interpreted as extension fractures or extensional faults, interrupts the chasma at 6:00. From 2:00 to 6:00, the trough displays an asymmetric slope and morphology; normal faults are developed along the inner steep slope, and folds have formed along the outer slope (Figs. 2 and 4). Chasma folds decrease in wavelength from the outer trough toward the trough axis. Along and within the trough axis, folds and faults are indistinguishable as individual lineaments and fall below data resolution, as noted by Brown and Grimm (1995). Fault-bend folds developed along the outer trough margin (Suppe and Connors, 1992) display left-stepping and right-stepping patterns at ~2:00 and 5:00, respectively, indicating that shortening was not exactly normal to the trough axis at these locations (Brown and Grimm, 1995). Normal faults typically step downward into the trough interior. Locally normal faults, which strike parallel to fold axes, likely cut folds as noted by Brown and Grimm (1995), although in many cases, data resolution does not allow robust feature identification or interpretation of temporal relationships.

Within parts of the chasma, extensional fractures or normal faults (graben of Brown and Grimm, 1995) trend perpendicular to the chasma folds. For brevity, the structures are referred to herein as ''fractures,'' although it is recognized that they comprise fractures, normal faults, and locally grabens. The fractures extend into the chasma from the exterior and locally to the interior (e.g., 5:00). In general, these structures, which are radial to the chasma, predate the folds (Brown and Grimm, 1995), although locally they could have been reactivated during or after fold formation. The fractures reflect topographic lows as indicated by local filling by younger surface flows (e.g., 40°S, 143°E), evidence that they record minor extension normal to their trend. Although Brown and Grimm (1995, their Fig. 12) suggested that these structures were distorted within the chasma by ~60% shortening perpendicular to fold crests, the region east of the strain measurements hosts at least two suites of fractures oriented parallel to their undistorted and ''distorted'' equivalents (Fig. 5). The apparent distortion results from combining two orientations of fractures (Fig. 5); thus, suggestions of 60% shortening are unsupported.

The western chasma fades at ~10:30 and, from there, widens and deepens in a counterclockwise fashion. At 9:00, three distinct suites of lineaments occur: Closely spaced northeast-trending fractures; more widely spaced northwest-trending paired fractures or grabens; and north-northwest–trending folds (Fig. 3B). Northeast-trending fractures formed prior to northwest-trending fractures and folds as evidenced by their spacing and distribution on either side of the fold belt. Northwest-trending fractures dominantly predate the folds, although some may have been reactivated after or during fold formation. Northeast-trending fractures occur on either side of the narrow chasma fold belt and are discernible at the fold crests with little (<5°) change in orientation, indicating that although the surface is downwarped at this location, the surface material has not been underthrust or removed.

At ~1:00, Brown and Grimm (1995) interpreted a region of 50–250 km of left-lateral shear within the chasma. They based this interpretation mainly on a correlation of a fine-scale penetrative (at the scale of observation) ''lattice'' fabric purported to be preserved in both the interior and exterior (their Fig. 14). At ~12:30 within the chasma, just north of their lattice fabric, an early-formed penetrative linear fabric traverses the trough with no clear evidence of significant left-lateral shear (Fig. 2). As suggested by Brown and Grimm (1995), much or all of the apparent left-lateral displacement could have resulted from extension associated with normal faults that strike parallel to the trough axis. At the location of the proposed displacement, the trough is ~80 km wide and hosts numerous trough-parallel normal faults (Brown and Grimm, 1995, their Fig. 14B). If zero extension is assumed across this 80-km-wide zone (contrary to the mapped normal faults), the maximum left-lateral displacement is ~100 km; given the presence of normal faults parallel to the trough, this estimate is a maximum value. Thus, 100% extension across the zone would yield a maximum left-lateral displacement of 50 km; 150% extension would result in the total apparent 100 km displacement, with no true left-lateral displacement. Additionally, if this region actually was the site of significant left-lateral shear, then the normal faults should strike ~30° from the trough axis (interpreted as parallel to the shear zone) rather than parallel to the trough axis as documented by Brown and Grimm (1995) and confirmed by mapping here. Thus, this part of the chasma may (or may not) record moderate (~50 km) left-lateral shear, but 250 km of displacement is unlikely.

The chasma is poorly defined from ~10:00 to 11:00. Normal faults and scarps associated with Quilla Chasma to the west and radial and concentric fractures associated with small coronae merge with Artemis-related structures. A relatively late local lava flow that emerged from Quilla Chasma structures flowed southward, locally covering radial flows from corona C5 within the interior of Artemis (discussed subsequently; Fig. 2). This flow is cut, in turn, by east-trending fractures that could be related to C5 or could represent reactivated structures.

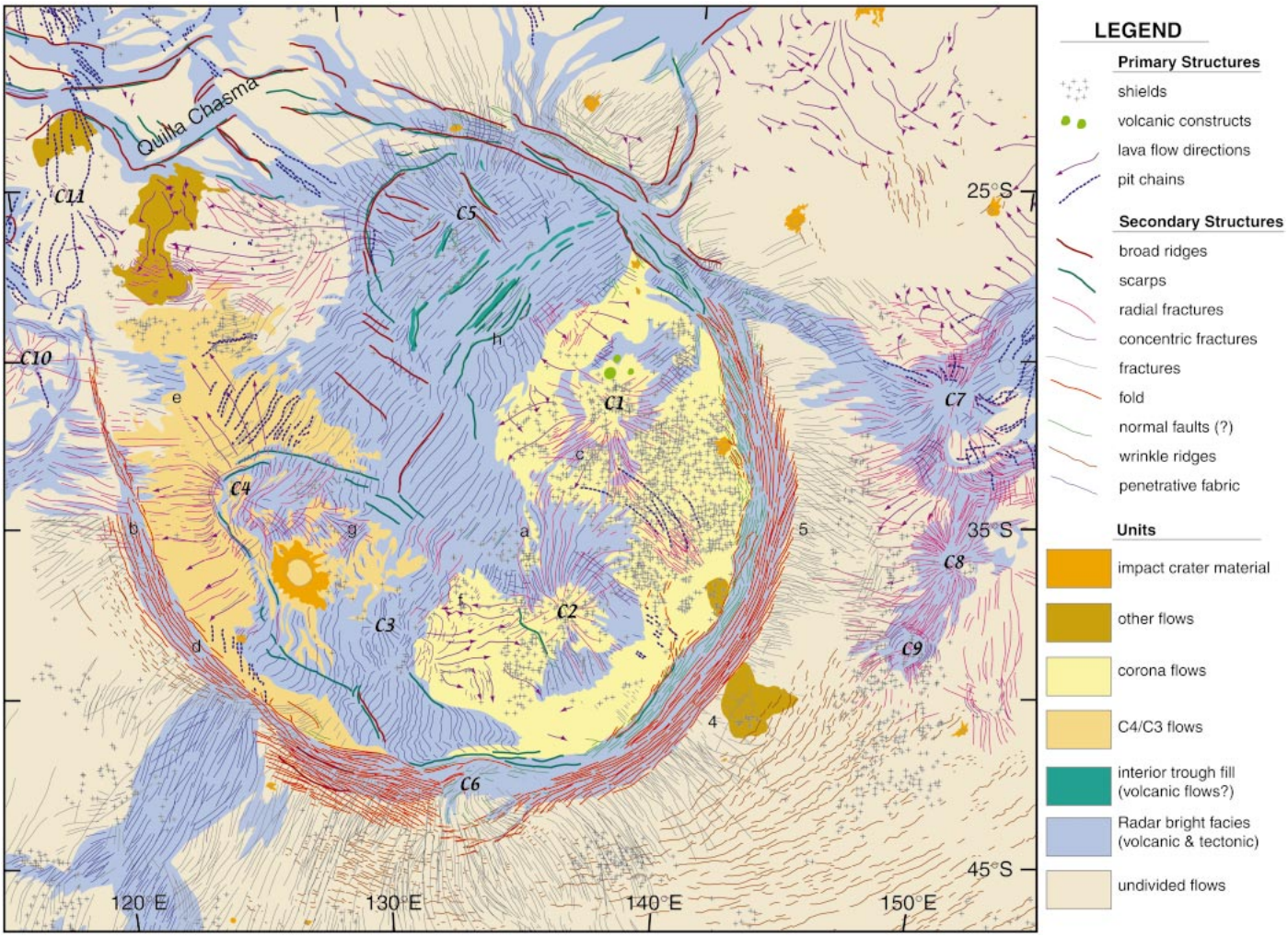

Figure 2. Geologic map of Artemis region (simplified from a compilation at 1:5 000 000 scale). Locations of Figure 3 images shown by letters; locations of Figures 4 and 5 shown by numbers; coronae C1–C11 labeled.

Brown and Grimm (1995) divided Artemis Chasma into five distinct regions—the northeast, east, southeast, south, southwest margins. Although differences in structural fabrics are preserved along the chasma, as has already been noted, the current analysis did not uncover any clear boundaries along the chasma (Fig. 2), nor do discontinuities appear in Brown and Grimm's tectonic map (1995, their Fig. 16). Most specifically there seems to be no evidence to suggest that the southern and southwestern parts of the chasma are distinct from the rest of the chasma. Chasma folds fade at ~10:00 and, from there, increase in intensity in a counterclockwise direction, and the width of the fold belt and fold spacing increase continuously along the chasma. At 7:00–8:00, the chasma fold belt narrows at a region spatially correlative with a northeast-trending exterior fracture zone. Temporal relationships between the chasma folds and the fracture zone are poorly determined. However, crustal anisotropy represented by the fracture zone could have influenced coherent formation of the chasma, and therefore the presence of the fracture zone should not be used to define fundamentally discrete regions of the chasma. Similarly, at 6:00, corona C6—marked by radial fractures—deflects chasma fold crests and faults, indicating that C6 was at least in part present while the chasma, folds, and faults formed. The strain partitioning that results from C6 is consistent with a mechanically heterogeneous crust, as would be expected for a tectonically active terrestrial planet. The difference in the chasma structure at the juncture with either the fracture zone or C6 does not provide robust evidence that different parts of the chasma formed at different times or represent fundamentally different geologic events as previously suggested.

Interior Features

The interior preserves five coronae or corona-like features defined by radial fractures and/or by concentric fractures or folds and radial lava flows, informally labeled C1–C5 (Fig. 2). The coronae, individually and collectively, record a rich history of spatially and temporally overlapping deformation (fractures, faults, folds) and volcanism. Small but numerous shields (e.g., Head et al., 1992; Addington, 2001) associated with each corona appear to have formed relatively late, but it may be that earlier-formed shields are simply not observable with current data resolution.

C1 is defined by several independent elements that describe a circular feature: (1) radial fractures centered about (2) a radar-dark region that hosts numerous shields and that is surrounded in turn by (3) a region of radar-bright facies and (4) outboard radial lava flows

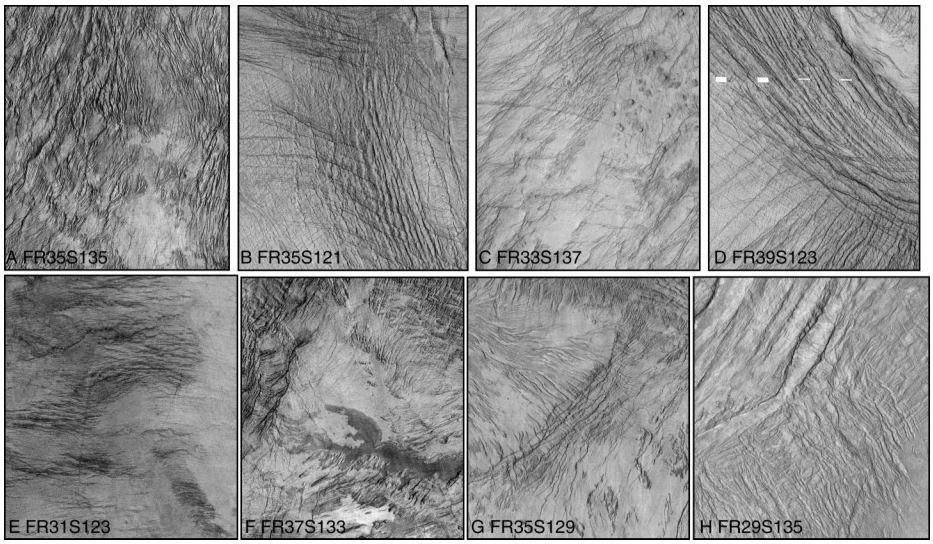

Figure 3. Negative SAR F-tile (full resolution), right-look (R) images of selected areas across Artemis. Tile-center location in each image labeled. Tile long dimension is ~200 km. Tile locations are shown by letters A–H in Figure 2; analogue clock–type directions refer to the whole structure shown in Figure 2. (A) Artemis radar brightness is locally a function of both tectonic and volcanic fabrics that can be difficult to delineate at the scale of the data. (B) Northeast-trending closely spaced fractures and younger, northwest-trending, more widely spaced fractures, deformed by north-northwest–trending fold crests at 9:00 within Artemis chasma. (C) Volcanic flows, locally with or as shields, form a thin layer that locally veils early-formed tectonic fabric. (D) At ~8:00 in Artemis, interior flows abut the chasma folds and are locally deformed by them. (E) Penetrative tectonic fabrics (horizontal features) are preserved as kipukas; the boundaries with younger lava surfaces (smooth areas) preserve details to the scale of data resolution. (F) Radar-bright and -dark flows from corona C3 that fill local structural topography resulting from penetrative tectonic fabric are cut by locally north-trending fractures concentric to C3. (G) Along the east side of corona C4, northeast-trending grabens cut earlier flows, which in turn variably cover an early-formed penetratively developed tectonic fabric. (H) An early-formed penetrative northeast-trending tectonic fabric (upper right) is cut by northwest-trending grabens (lower right), which are in turn cut by spaced, northeast-trending scarps or ridges (upper left).

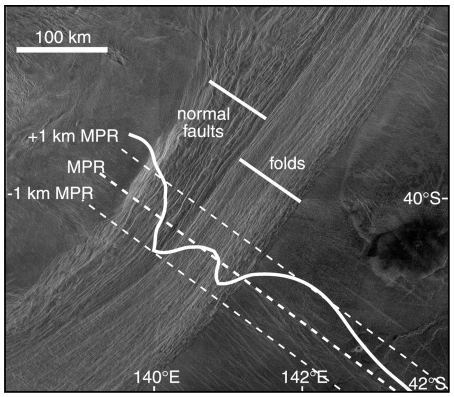

Figure 4. SAR image of part of southeast Artemis Chasma with topographic profile along transect shown (i.e., the MPR line). Normal faults are developed along the steep in-trench slope; folds are developed along the more gently sloping outer-trench slope. Topographic profile after Brown and Grimm (1996) with 25× vertical exaggeration.

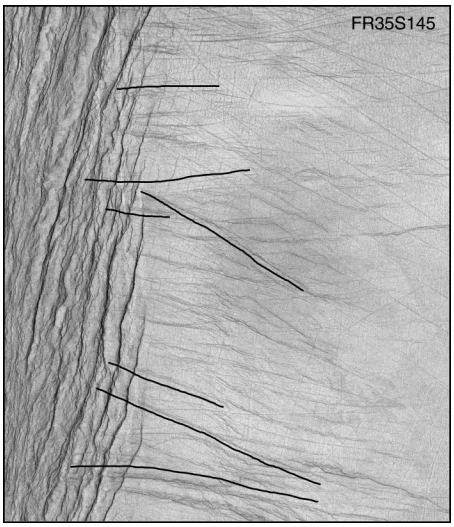

Figure 5. Negative right-look SAR F-tile centered at 35°S, 145°E shows at least two orientations of fractures west of Artemis chasma. The apparent deflection of fractures within the chasma by chasma folds results from the (incorrect) association of different parts of separate fracture suites; individual fractures are not deflected by folds along their trace, as shown by the black lines, which parallel, but are offset from, the fracture trace, allowing the reader to follow the continuity of individual fractures.

that flow away from C1 toward C3/C4 and C5. Radial fractures are also preserved within and cut the radar-bright facies. Three small volcanic structures lie along the north side of C1. Volcanic flows form a thin layer that locally veils early-formed tectonic fabrics (Fig. 3C). Shields, likely related to C1, are cut by inboard normal faults at ~32°S, 142°E. At C2, located south of C1, radial fractures variably cut both the radar-bright facies and parts of the flooded and/or shield-bearing interior. C2 also displays northwest-trending fractures and scarps.

C3 and C4 might be considered a double corona with C3 subsidiary to C4. Radial fractures, concentric fractures and scarps, and radial lava flows define the center of C4, an elliptical corona with C3 forming a focus marked by faint radial fractures, and concentric fractures and radial flows developed along its eastern side (Fig. 2). Radial flows that emanate from C4 flow to the southwest and northwest, locally covering earlier-formed radial fractures, yet also cut by radial fractures (Fig. 6). In addition, the flows are cut by northeast-trending fractures and pit chains (Okubo and Martel, 1998) that parallel the trend of the tectonic fabric in the underlying radar-bright facies. The northeast boundary of these flows clearly indicates that the flows postdate the formation of the radar-bright facies at this location, but contact relationships along the southwest margin of the flow are less obvious. At ~9:00–8:00, the interior flows appear to abut the chasma folds and to be locally deformed by them (Figs. 3D, 6). Fractures radial to C4 apparently cross, and are cut by, the chasma fold belt at 9:00–10:00; locally flows cover the radial fractures, although other radial fractures cut the flows.

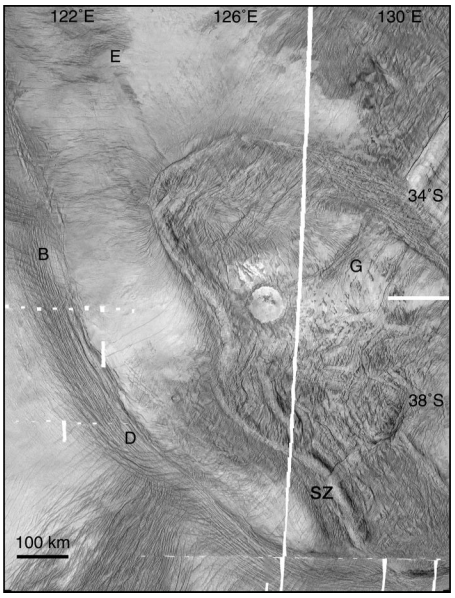

Figure 6. C1-negative SAR image of corona C4 in the southwest interior of Artemis. Fractures radial to C4 are cut by chasma folds and locally covered by flows radial to C4; yet lava flows from C4 are locally buttressed by chasmata folds (see also Fig. 3D), and late radial fractures cut C4 flows. Locations of B, D, E, and G in Figure 3 are shown by letters; sz indicates location of the "right-lateral shear zone" of Brown and Grimm (1995); this zone can be interpreted as part of the annulus to C4/C3. Circular feature in the middle of the image is an impact crater.

Tectonic fabrics, penetrative at the scale of observation, are preserved locally; the boundaries with younger lava surfaces preserve details of the scale of data resolution (Fig. 3E). Radar-bright and -dark flows from C3 that fill local structural topography resulting from penetrative tectonic fabric are cut by locally north-trending fractures concentric to C3 (Fig. 3F). Taken together, these features reflect a complex tectono-volcanic history of C4/C3 and suggest that corona evolution overlapped in time with formation of Artemis Chasma from 6:30–10:00. Similar interrelated tectono-volcanic relationships are preserved on the east side of C4 where northeast-trending grabens cut earlier flows, which in turn variably cover an early-formed penetratively developed tectonic fabric (Fig. 3G). Each of the coronae also hosts numerous small volcanic shields. Shields generally range from 2 to 10 km across and are probably <0.5 km high (Kreslavsky and Head, 1999, Addington, 2001). The shields occur extensively in places across the radar-bright facies, as well as within and across the radar-dark facies. Individual shields, which can be either radar-dark or -bright, overprint and are cut by local tectonic structures; thus, tectonism and volcanism overlapped in time. The most obvious shields are, of course, those that represent the youngest local features, but this observation indicates more about preservation than about strict relative temporal relationships. Pit chains, which probably represent magma at depth with local magma erosion to the surface (Okubo and Martel, 1998), generally parallel the trends of local tectonic fabric and provide evidence of relatively late magmatic activity.

The interior of C4/C3 comprises Spencer's (2001) southern interior deformation belt (his Fig. 2), and the southwestern scarp of C4/C3 represents the interior north-northwest–trending deformation belt of Brown and Grimm (1995, their Fig. 9). The combination of concentric folds, ridges, faults, and scarps defines an asymmetric annulus to coronae C4/C3 (Figs. 2 and 6). Brown and Grimm (1995, p. 233) postulated right-lateral shear along the southwest part of the annulus on the basis of the "discrete fault (scarp) and en echelon graben[s]." The "en echelon graben[s]" could simply represent deflection of radial fractures along the asymmetric C4/C3 corona annulus (Figs. 2 and 6). Spencer (2001) interpreted the northeast part of the annulus as a right-lateral shear zone and stated that the penetrative tectonic fabric ends abruptly at this zone and exists only to the north. However, the penetratively developed northeast-trending tectonic fabric extends for some distance on either side of both the southwest and northeast scarps, indicating a general continuity of the surface across the annulus and scarps and that the penetrative tectonic fabric predated annulus and scarp formation (Figs 2 and 6; Brown and Grimm, 1995, their Fig. 9; Spencer, 2001, his Figs. 2–4).

The northernmost corona feature, C5, is the least corona-like. The radar-bright facies dominates C5, although local radial fractures, concentric fractures, and scarps and radial flows developed along the northwest margin of C5 lead me to classify it as a corona. C5 encompasses much of the northeastern interior deformation belt of Spencer (2001) and includes northeast-trending ridges, scarps, and lava-flow-filled valleys. C5 probably records the most complex history of the interior coronae; some of its history may predate formation of the radial flows and concentric fractures and scarps, attributed to corona formation. Fractures radial to C5 extend across the chasma at ~11:00–1:00, although it is difficult to determine whether these structures represent a genetically related structure suite. Parts of C5 record many episodes of deformation; for example, at location H (Fig. 2), an early-formed penetrative northeast-trending tectonic fabric is cut by northwest-trending graben, which are in turn cut by spaced northeast-trending scarps or ridges (Fig. 3H). Locally, lava flows fill the valleys, interpreted as rift-related graben (Brown and Grimm, 1995; Spencer, 2001). The variable muted to sharp preservation of the tectonic fabric across much of C5 might be due to local volcanism similar to that preserved elsewhere (Fig. 3, A, C, G).

In summary, five coronae, which individually and collectively record intimately related tectonism and volcanism, dominate the interior of Artemis. Although Brown and Grimm (1995) defined the interior lava flows as "interior volcanic plains" and subsequently inferred a temporal correlation to "exterior plains," these flows are likely corona-derived flows, and no direct evidence correlates them with exterior "plains." Although there may be remnants of early-formed "plains," one cannot point to any specific region that cannot be attributed to either the multiphase radar-bright facies or to coronae.

Exterior Features

The region outside Artemis Chasma is quite varied. The region to the north (outside the map area) includes part of the crustal plateau Thetis Regio, which is locally overprinted by coronae, and fractures associated with Kuanja, Virava, Quilla, and Diana chasmata. Several small coronae may mark the termination of Dali and Juno chasmata, to the east and west of Artemis, respectively. South from ~4:00 to 9:00, the exterior is notably free of coronae or fractures, except for the ~400-km-wide fracture zone at ~7:00 and C6 within the chasma at 6:00. Trough-normal fractures or grabens and trough-parallel wrinkle ridges are variably developed outboard of the chasma. Fractures are preserved over ~320° (or more) from ~11:00 clockwise to ~9:30. Chasma and chasma folds locally overprint the radial fractures as illustrated by Brown and Grimm (1995) and confirmed by mapping presented here. Overprinting relationships are documented from 2:00 to 10:00 (and possibly to 1:00) within the chasma (Fig. 2). However, as previously noted, there is no clear evidence that chasma folds distort the fractures. Trough-concentric wrinkle ridges generally lie farther outboard of the radial fractures and are preserved at ~2:00, and from 4:00 to 9:00, except within the fracture zone at 7:00.

The radial fractures, wrinkle ridges, or both are locally either not preserved or never formed. For example, at 4:30 just outboard of the chasma (40°S, 143°E), radial fractures are not obvious (Brown and Grimm, 1995). However, close examination of SAR imagery indicates that postfracturing lava flows locally cover the fractures, providing evidence that radial fractures originally formed at this location, that the fractures are topographic valleys, and that local exterior volcanism postdates some radial fracture formation. At 2:00–4:00, wrinkle ridges are not present outboard of the chasma. However, within this region, small coronae, C7–C9, dominate the tectonic fabric (Fig. 2). Flows from the coronae locally cover Artemis-related radial fractures, but elsewhere Artemis-related radial fractures may cut flows related to these coronae. Because coronae record complex tectono-volcanic histories (e.g., Baer et al., 1994; Copp et al., 1998; Guest and Stofan, 1999; Rosenberg and McGill, 2001; Hansen and DeShon, 2002) and because structures can be reactivated, one should not interpret local lava-flow and fracture relationships as evidence of robust temporal relationships between outboard coronae and Artemis. Several interpretations are valid: (1) If the coronae predated Artemis, then wrinkle ridges might not have formed along this region of anisotropic crust. (2) If coronae postdated Artemis, then earlier-formed wrinkle ridges could have been buried or destroyed. (3) If the coronae formed broadly contemporaneously with Artemis, then the local crustal environment or stress regime might not have favored wrinkle-ridge formation. Thus, the lack of wrinkle ridges along this region does not differentiate between models of Artemis's formation, nor does it set limits on temporal relationships between Artemis and outboard coronae.

Wrinkle ridges are also absent outboard of the chasma at ~7:00 where the northeast-trending fracture zone intersects the chasma. Relative temporal relationships between the fracture zone and chasma are so far undefined. Although Brown and Grimm (1995, p. 242) indicated that crosscutting relationships support an interpretation that the fracture zone (''rift'' in their terminology) is younger, they did not elaborate (furthermore, the image cited by Brown and Grimm does not include the fracture zone or the region southwest of the chasma). Numerous small volcanic shields occur along and within the fracture zone. On the basis of reasoning similar to that already presented herein, it is not clear (1) whether these shields cover earlier-formed wrinkle ridges, (2) whether wrinkle ridges never formed at this location because of an earlier-imposed fracture-zone anisotropy, or (3) whether the fracture zone and Artemis formed contemporaneously. Given that fracture zones display interrelated tectonic and volcanic histories (Bleamaster and Hansen, 2001; Hansen and DeShon, 2002) and given that Artemis records a complex tectonic history, it is dangerous to use a single temporal relationship, or even a small suite of locally preserved temporal relationships, to extrapolate local temporal constraints to regional scales.

GEOHISTORY INTERPRETATION

Although the geologic map presented here is generally consistent with that of Brown and Grimm (1995), I propose a different geologic history related to three fundamental differences in interpretation. (1) Artemis Chasma formed as a coherent entity rather than as separate features, as evidenced by the continuity of the chasma and chasma structures illustrated both in the map herein (Fig. 2) and that of Brown and Grimm (1995, their Fig. 16). (2) Related to item 1, the radial fractures and concentric wrinkle ridges outboard of the trough formed broadly contemporaneously with the chasma and chasma structures and are genetically related to trough formation. (3) Part (if not all) of the interior tectonic fabric and lava flows are related to interior corona formation, and these coronae formed during Artemis evolution and do not record widespread, early ''plains'' volcanism or ''captured real estate'' (e.g., Brown and Grimm, 1995; Hansen et al., 1997).

Chasma folds and normal faults, chasma-normal fractures, and outboard chasma-concentric wrinkle ridges can all be interpreted within a coherent tectonic framework consistent with temporal and spatial relationships gleaned from available *Magellan* data sets. These structures describe coherent patterns *relative to the chasma* along the length of the chasma; specifically, (1) folds or normal faults everywhere parallel the trend of the chasma; normal faults generally occur inboard of folds where both occur along the same length of the chasma; (2) fractures strike perpendicular to the chasma at all points along it; (3) exterior wrinkle ridges trend parallel to (or concentric to) the trend of the local chasma; and (4) each of these elements—chasma, folds, normal faults, fractures, and wrinkle ridges—independently define circular features whose centers all lie within the same general region in the center of Artemis (Fig. 7). Such spatial correlation is consistent with a genetic relationship among these diverse geomorphic and structural features. Local relationships can explain local deviations from these general patterns, as already discussed. Thus, it is viable to conclude that Artemis Chasma and its folds and normal faults represent a coherent tectonic feature that formed contemporaneously with radial fractures and concentric wrinkle ridges.

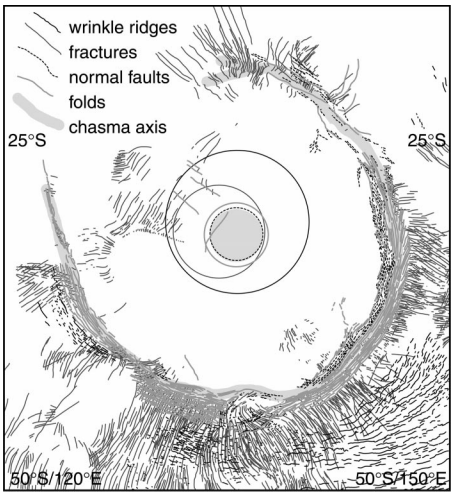

Figure 7. Map illustrating spatial correlation of the centers of the circles defined by various topographic and structural elements associated with Artemis.

In contrast, Brown and Grimm (1995) proposed that the southeastern, eastern (2:00–6:00), and northeastern (12:00–2:00) parts of Artemis Chasma formed as a result of northwest-directed underthrusting and related left-lateral shear, respectively, and that the southern, southwestern and western parts of Artemis Chasma (6:00–10:00) formed during earlier unrelated event(s).

The current study indicates that much of the radar-dark, and hence smooth, regions previously interpreted as ancient plains (Brown and Grimm, 1995; Hansen et al., 1997), represent regions of relatively recent volcanism (although there are also numerous locations where local tectonism outlasted volcanism); thus, these surfaces are relatively young rather than old. Furthermore, interior volcanic flows relate to corona formation rather than ancient volcanic plains. Although some of the deformed material within the radar-bright facies could in part represent ancient ''plains,'' there is no direct evidence to support this interpretation. Even if a part of the interior could be shown to preserve robust evidence of ancient plains, such preservation could be accommodated in a wide range of models of Artemis evolution (including the model proposed herein).

Additionally, relationships noted herein indicate broadly contemporaneous development

of the interior and the chasma. Fractures radial to C5 and C4/C3 are locally cut by folds in the western chasma, yet volcanic flows associated with C4/C3 cover these radial fractures and are locally buttressed by chasma folds. Finally, fractures radial to C4 cut these flows. Similar arguments can be made for each interior corona; thus, broadly contemporaneous formation of the Artemis interior and the chasma are permissible by the current data, whereas proposals that the interior formed prior to the chasma are unsupported.

Spencer (2001) postulated that the center of Artemis represents the grooved surface of a 300 by 300 km molded footwall of an extensive extensional system; he argued that northwest-trending grooves formed as a result of plastic molding of the footwall by irregularities on the underside of the hanging wall. However, the penetrative fabric trends northeast across this region (his Fig. 3). Although Spencer stated that the northeast-trending fabric terminates at his ''en echelon zone'' and thus formed after the northwest-trending ''grooves,'' this statement is not supported by SAR imagery (his Figs. 3 and 4), my mapping (Fig. 2), or the mapping of Brown and Grimm (1995). The northeast-trending fabric extends across the en echelon zone to the south and is also contiguous with a similar fabric to the north (Fig. 2). The regional development and the tight-spacing and along-strike character of the northeast-trending fabric are more easily reconciled with early formation of this fabric.

Collectively, I interpret that exterior radial fractures—locally overprinted by chasma-parallel folds—formed owing to broad radial extension centered on Artemis. Early (and locally continuing) radial extension was followed by formation of local interior coronae and the entire Artemis Chasma. Within this context the chasma, folds, normal faults, radial fractures, and concentric wrinkle ridges display a kinematically consistent pattern across Artemis; there is no need to infer distinct geologic events for any of these elements or for different parts of the chasma. The circular nature of the chasma and the continuity and similarity of structures along the chasma argue against a two-phase and serendipitous alignment of detailed tectonic structures.

ARTEMIS EVOLUTION

The major features of Artemis—broad topographic signature, evidence of interior extension, circular topographic trough, concentric contractional and extensional trough structures, radial fractures, and exterior concentric wrinkle ridges—can be accommodated within the spirit of the mantle-plume models of Artemis formation proposed previously (Herrick and Phillips, 1990; Griffiths and Campbell, 1991; Sandwell and Schubert, 1992). Although the models may require some modification, the general proposal that Artemis represents the surface signature of a large mantle diapir on the lithosphere not only is permissible, it is strongly supported by geologic relationships. Herrick and Phillips (1990) first suggested a diapiric (so-called ''blob'') interpretation for Artemis (and Ovda, Thetis, and Beta Regiones) prior to the acquisition of *Magellan* data. Although I favor the spirit of their model, the original postulated stages of evolution are not supported by *Magellan* data (see discussion in Phillips and Hansen [1994] and Hansen et al., [1997]), but neither are such stages required by a diapir model. The size and circular shape of Artemis are consistent with formation by the interaction of a deep mantle plume on the lithosphere. Gravity-topography analysis is consistent with at least partial dynamical support for Artemis (Simons et al., 1997). As a deep mantle plume rises toward a lithosphere, the lithosphere will be uplifted, and, if the strength of the lithosphere is exceeded, radial fractures could form above the plume head. A circular trough could also form, as illustrated in laboratory experiments aimed at modeling the interaction of thermal plumes with the lithosphere (Griffiths and Campbell, 1991). In these experiments, as a plume head approaches a rigid horizontal boundary, it collapses and spreads laterally; a layer of surrounding mantle is squeezed out from between the plume and the surface, resulting in a gravitationally trapped asymmetric instability and formation of an axisymmetric trough. In addition, the interior squeeze layer can lead to convection on a scale much smaller than that of the original plume. These smaller-scale instabilities could interact with the lithosphere inside the axisymmetric trough. It was on the basis of Griffiths and Campbell's experiments that a plume model for Artemis formation was proposed following release of *Magellan* data (Griffiths and Campbell, 1991). Finite-element models of the interaction of a thermal plume with a lithosphere, aimed at modeling corona topography, also show development of an axisymmetric trough above large thermal mantle plumes (Smrekar and Stofan, 1997). Smrekar and Stofan (1997) applied their model to coronae; however, their model provides a better analogue for Artemis because their resulting trough-to-trough diameter is >1200 km—much larger than median coronae (200 km diameter) (Stofan et al., 1992).

The chasma structures could also form during the plume-lithosphere interaction. Within the trough, material is pulled downward, resulting in the formation of folds and normal faults at the surface (Smrekar and Stofan, 1997). One can envision a range of deformation that could be preserved within such a trough, including (1) minor contraction with preservation of the earlier-formed surface features such as at 9:00 within the trough (Fig. 3B); (2) dominant extension of the trough surface marked by trough-parallel normal faults (e.g., at 12:30–1:30); and (3) shortening and extension within the trough, perhaps resulting from inward or outward movement of the trough during plume evolution. Outward movement of the trough might be expected to result in normal faults developed along a steep inner slope and folds developed along the outer slope (and leading edge of the trough) of the chasma as documented from 2:00 to 6:00 (Figs. 2, 4). The trough could also show a topographic asymmetry as developed in the finite-element model of Smrekar and Stofan (1997). The asymmetry of the axisymmetric trough (i.e., steep slope along the inner trough) as well as the angle of downwelling beneath the plume head formed within Smrekar and Stofan's (1997) model is consistent with both the topographic asymmetry of Artemis Chasma from 3:00 to 5:00 and the distribution of normal faults and folds within the chasma.

Thus, each of the major elements that define circular features associated with Artemis can be accommodated within a model involving a deep mantle plume. Rising and flattening of the plume head led to early uplift and doming of the surface and the formation of radial fractures. As the plume head collapsed vertically and spread laterally, a squeeze layer was trapped, and an axisymmetric trough formed. Both the trough (chasma) and the trough structures could have deformed early-formed radial fractures. Spreading of the plume laterally outboard of the trough might have resulted in continued radial-fracture formation and development of contractional structures (wrinkle ridges) concentric to the trough and plume head. The region interior to the topographic trough could have been affected by small-scale convection cells or compositional diapirs resulting in local corona-like structures with radial fractures, and/or concentric fractures or folds, and associated volcanism.

In arguing against a mantle-diapir interpretation for Artemis, Brown and Grimm (1995, p. 245) stated that a diapiric model for Artemis formation would require ''interior radially *symmetric* shortening.'' However, although

both empirical and finite-element modeling of diapiric structures show interior radial shortening, neither requires interior radially *symmetric* shortening even if a plume interacts with a homogeneous lithosphere (e.g., Withjack and Scheiner, 1982; Griffiths et al., 1989; Griffiths and Campbell, 1991; Moore et al., 1999). A heterogeneous lithosphere would lead to less symmetry. Although the interior of Artemis indeed lacks evidence of radial axisymmetric shortening, the distribution of mostly exterior radial fractures and concentric wrinkle ridges display evidence of regionally developed quasi-axisymmetric shortening (Figs. 2 and 7).

Brown and Grimm (1995, p. 245) further stated that Artemis ''chasma has mainly experienced convergence and horizontal shear rather than extension.'' Two points are relevant to consider (Brown and Grimm, 1995, their Fig. 16) (Fig. 2). (1) Contraction within the chasma, preserved along ~200°, is concentric to the chasma—not limited to the southeast margin as emphasized by Brown and Grimm (1995). (2) The chasma preserves evidence of both extension and shortening; both could occur in an axisymmetric trough formed as a result of the interaction of a large diapir with a lithosphere (e.g., Griffiths and Campbell, 1991; Smrekar and Stofan, 1997). Therefore, a diapir model for Artemis cannot, and should not, be dismissed. Emphasized by Brown and Grimm (1995) also argued against coherent formation of the chasma and its structures because they could not accommodate all of the chasma deformation into a model of 250 km of northwest-directed underthrusting beneath Artemis, which they proposed for the eastern part of the chasma. Such reasoning is circular. In addition, the underthrusting model encounters problems in light of recent mapping, as follows.

1. ''Upper-plate'' volcanism—represented by the interior volcanic flows, shields, and pit chains—would not be expected in the underthrusting model because of a depressed thermal gradient. Terrestrial arc volcanism results from water fluxing and the resulting melting-point depression, but Venus's anhydrous rock lacks water for fluxing (Kaula, 1990).

2. The underthrusting model does not address the remarkable continuity of chasma structures and structural patterns relative to chasma location. Few geologic features define remarkably circular features as a result of serendipitous alignment of unrelated events.

3. The locations of chasma folds and normal faults are not entirely consistent, and are arguably inconsistent, with the underthrusting model. Assuming that the chasma is analogous to a terrestrial subduction trench, the chasma normal faults and folds from 3:00 to 6:00 are located opposite from where one would predict. Normal faults occur on the leading edge of the postulated ''upper-plate,'' whereas chasma folds occur along the bend of the downgoing ''plate'' (Fig. 4). Furthermore, the overall width of the deformed belt (~150 km) would seem to suggest steep underthrusting, yet such an inference is contrary to the development of a trough over an ~100° arc with a diameter of ~2100 km, which would imply shallow underthrusting.

4. If the northeast margin (12:00–2:00) recorded the postulated significant left-lateral shear, then normal faults should strike at ~30° from the trough axis (interpreted as a parallel to the shear zone), rather than trend parallel to the trough axis.

5. Finally, as noted (Brown and Grimm, 1995), the exterior fractures would be expected to form concentric to the outer high, rather than perpendicular as documented.

Following Brown and Grimm (1995), Spencer (2001) postulated that the center of Artemis represents the grooved surface of a 300 by 300 km molded footwall of an extensive extensional system. He argued that northwest-trending grooves formed as a result of plastic molding of the footwall by irregularities on the underside of the hanging wall. However, the penetrative fabric trends northeast across this region and likely formed prior to Spencer's ''grooves'' and ''en echelon zone''; thus this fabric is difficult to reconcile with molding of a ductile footwall.

IMPLICATIONS AND CONCLUSIONS

Venusian crustal plateaus and volcanic rises, which define quasi-circular structures similar in size to Artemis, also represent the surface signature of large mantle plumes (Hansen and Willis, 1998; Phillips and Hansen, 1998; Hansen et al., 1999, 2000). Differences in geophysical signature, topographic profile, surface structural patterns, and geologic histories of plateaus and rises reflect differences in global lithospheric thickness during the time of plateau and rise formation; crustal plateaus formed in ancient thin lithosphere, whereas volcanic rises formed in contemporary thick lithosphere. Phoebe Regio, a unique feature that has some plateau and some rise characteristics, is proposed to have formed during the transition from thin to thick lithosphere. Artemis also appears to represent a transitional form of a plume signature, probably formed in late thin-lithosphere time, prior to formation of Phoebe Regio. The very short wavelength or closely spaced penetrative tectonic fabric across Artemis might be consistent with deformation of an extremely thin layer and thus perhaps indicate a very shallow depth to the local brittle-ductile transition during the development of these fabrics. In contrast, Phoebe Regio preserves a much less penetratively developed fabric (Hansen and Willis, 1996), consistent with a thicker brittle (strong) layer and hence perhaps a deeper regional brittle-ductile transition. If the thermal energy transported by all Venusian deep mantle plumes is grossly similar and if the Venusian lithospheric composition is approximately uniform, then differences in the depth to the brittle-ductile transition across a region affected by a plume would be a function of lithospheric thickness; possible temporal relationships between Phoebe Regio and Artemis require further study. On the basis of data presented herein, Artemis likely represents the surface signature of a deep mantle plume on the surface of Venus, and Artemis probably formed at, and thus records, a relatively unique time in the evolution of Venus's lithosphere.

ACKNOWLEDGMENTS

This work was supported in part by U.S. National Aeronautics and Space Administration grants NAG5-4562 and NAG5-10586. Discussions with, and comments by, V. Bennett, I. Campbell, G. Davies, D. DePaolo, J. Goodge, R. Griffiths, C. Meriaux, and S. Turner were extremely helpful, but any omissions or oversights are mine. This work grew out of a research sabbatical at the Australia National University (ANU), funded by Southern Methodist University and hosted by ANU. I thank the staff at both institutions for making my visit possible, and J. Stamatakos and D. Ferrill for helpful reviews.

REFERENCES CITED

Addington, E.A., 2001, A stratigraphic study of small volcano clusters on Venus: Icarus, v. 149, p. 16–36.

Baer, G., Schubert, G., Bindschadler, D.L., and Stofan, E.R., 1994, Spatial and temporal relations between coronae and extensional belts, northern Lada Terra, Venus: Journal of Geophysical Research, v. 99, p. 8355–8369.

Bleamaster, L.E., III, and Hansen V.L., 2001, The Kuanja/Vir-Ava Chasmata: A coherent intrusive complex on Venus: Houston, Texas, Lunar and Planetary Institute, Lunar and Planetary Science Conference XXXII, Adobe Acrobat computer file 1316.pdf.

Brown, C.D., and Grimm, R.E., 1995, Tectonics of Artemis Chasma: A Venusian ''plate'' boundary: Icarus, v. 117, p. 219–249.

Brown, C.D., and Grimm, R.E., 1996, Lithospheric rheology and flexure at Artemis Chasma, Venus: Journal of Geophysical Research, v. 101, p. 12697–12708.

Brown, C.D., and Grimm, R.E., 1999, Recent tectonic and lithospheric thermal evolution of Venus: Icarus, v. 139, p. 40–48.

Copp, D.L., Guest, J.E., and Stofan, E.R., 1998, New insights into corona evolution: Mapping on Venus: Journal of Geophysical Research, v. 103, p. 19401–19410.

Ford, J.P., Plaut, J.J., Weitz, C.M., Farr, T.G., Senske, D.A.,

Stofan, E.R., Michaels, G., and Parker, T.J., 1993, Guide to *Magellan* image interpretation: National Aeronautics and Space Administration Jet Propulsion Laboratory Publication: Pasadena, California, JPL Publication 93–24, 148 p.

Ghent, R.R., and Hansen, V.L., 1999, Structural and kinematic analysis of eastern Ovda Regio, Venus: Implications for crustal plateau formation: Icarus, v. 139, p. 116–136.

Griffiths, R.W., and Campbell, I.H., 1991, Interaction of mantle plume heads with the Earth's surface and onset of small-scale convection: Journal of Geophysical Research, v. 96, p. 18295–18310.

Griffiths, R.W., Gurnis, M., and Eitelberg, G., 1989, Holographic measurements of surface topography in laboratory models of mantle hotspots: Geophysical Journal, v. 96, p. 477–495.

Guest, J.E., and Stofan, E.R., 1999, A new view of the stratigraphic history of Venus: Icarus, v. 139, p. 55–66.

Hansen, V.L., 2000, Geologic mapping tectonic planets: Earth and Planetary Science Letters, v. 176, p. 527–542.

Hansen, V.L., and DeShon, H.R., 2002, Geologic map of Diana Chasma quadrangle (V-37), Venus: U.S. Geological Survey Geologic Investigations Series Map I-2752, scale 1:5 000 000, in press.

Hansen, V.L., and Phillips, R.J., 1995, Formation of Ishtar Terra, Venus: Surface and gravity constraints: Geology, v. 23, p. 292–296.

Hansen, V.L., and Willis, J.J., 1996, Structural analysis of a sampling of Tesserae: Implications for Venus geodynamics: Icarus, v. 123, p. 296–312.

Hansen, V.L., and Willis, J.J., 1998, Ribbon terrain formation, southwestern Fortuna Tessera, Venus: Implications for lithosphere evolution: Icarus, v. 132, p. 321–343.

Hansen, V.L., Willis, J.J., and Banerdt, W.B., 1997, Tectonic overview and synthesis, *in* Bouger, S.W., Hunten, D.M., and Phillips, R.J., eds., Venus II: Tucson, University of Arizona Press,p. 797–844.

Hansen, V.L., Banks, B.K., and Ghent, R.R., 1999, Tessera terrain and crustal plateaus, Venus: Geology, v. 27, no. 12, p. 1071–1074.

Hansen, V.L., Phillips, R.J., Willis, J.J., and Ghent, R.R., 2000, Structures in Tessera terrain, Venus: Issues and answers: Journal of Geophysical Research, v. 105, p. 4135–4152.

Head, J.W., Crumpler, L.S., Aubele, J.C., Guest, J.E., and Saunders, R.S., 1992, Venus volcanism: Classification of volcanic features and structures, associations, and global distribution from *Magellan* data: Journal of Geophysical Research, v. 97, p. 13153–13197.

Herrick, R.R., and Phillips, R.J., 1990, Blob tectonics: A prediction for western Aphrodite Terra, Venus: Geophysical Research Letters, v. 17, p. 212–2132.

Herrick, R.R., and Phillips, R.J., 1992, Geological correlations with the interior density structure of Venus: Journal of Geophysical Research, v. 97, p. 16017–16034.

Kaula, W.M., 1990, Venus: A contrast in evolution to Earth: Science, v. 247, p. 1191–1196.

Keep, M., and Hansen, V.L., 1994, Structural evolution of Maxwell Montes, Venus: Implications for Venusian mountain belt formation: Journal of Geophysical Research, v. 99, p. 26015–26028.

Kirk, R., Soderblom, L., and Lee, E., 1992, Enhanced visualization for interpretation of *Magellan* radar data: Journal of Geophysical Research, v. 97, p. 16371–16380.

Kreslavsky, M.A., and Head, J.W., 1999, Morphometry of small shield volcanoes on Venus: Implications for the thickness of regional plains: Journal of Geophysical Research, v. 104, p. 18925–18932.

Moore, W.B., Schubert, G., and Tackley, P.J., 1999, The role of rheology in lithospheric thinning by mantle plumes: Geophysical Research Letters, v. 26, p. 1073–1076.

Okubo, C.H., and Martel, S.J., 1998, Pit crater formation on Kilauea volcano, Hawaii: Journal of Volcanology and Geothermal Research, v. 86, p. 1–15.

Phillips, R.J., and Hansen, V.L., 1994, Tectonic and magmatic evolution of Venus: Annual Reviews of the Earth and Planetary Sciences, v. 22, p. 597–654.

Phillips, R.J., and Hansen, V.L., 1998, Geological evolution of Venus: Rises, plains, plumes and plateaus: Science, v. 279, p. 1492–1497.

Rosenberg, E., and McGill, G.E., 2001, Geologic map of the Pandrosos Dorsa (V5) Quadrangle, Venus: U.S. Geological Survey Miscellaneous Geological Investigations Series Map I-2721, scale 1: 5 000 000.

Rosenblatt, P., and Pinet, P.C., 1994, Comparative hypsometric analysis of Earth and Venus: Geophysical Research Letters, v. 21, p. 465–468.

Sandwell, D.T., and Schubert, G., 1992, Flexural ridges, trenches and outer rise around Venus coronae: Journal of Geophysical Research, v. 97, p. 15923–15948.

Sandwell, D.T., Johnson, C.L., and Suppe, J., 1997, Driving forces for limited tectonics on Venus: Icarus, v. 129, p. 232–244.

Schubert, G., Moore, W.B., and Sandwell, D.T., 1994, Gravity over coronae and chasmata on Venus: Icarus, v. 112, p. 130–146.

Simons, M., Solomon, S.C., and Hager, B.H., 1997, Localization of gravity and topography: Constraints on the tectonics and mantle dynamics of Venus: Geophysical Journal International, v. 131, p. 24–44.

Smrekar, S.E., and Stofan, E.R., 1997, Corona formation and heat loss on Venus by coupled upwelling and delamination: Science, v. 277, p. 1289–1294.

Spencer, J., 2001, Possible giant metamorphic core complex at the center of Artemis Corona, Venus: Geological Society of America Bulletin, v. 113, p. 333–345.

Squyres, S.W., Janes, D.M., Baer, G., Bindschadler, D.L., Schubert, G., Sharpton, V.L., and Stofan, E.R., 1992, The morphology and evolution of coronae on Venus: Journal of Geophysical Research, v. 97, p. 13611–13634.

Stofan, E.R., Sharpton, V.L., Schubert, G., Baer, G., Bindschadler, D.L., Janes, D.M., and Squyres, S.W., 1992, Global distribution and characteristics of coronae and related features on Venus: Implications for origin and relation to mantle processes: Journal of Geophysical Research, v. 97, p. 13347–13378.

Stofan, E.R., Hamilton, V.E., Janes, D.M., and Smrekar, S.E., 1997, Coronae on Venus: Morphology and origin, *in* Bouger, S.W., Hunten, D.M., and Phillips, R.J., eds., Venus II: Tucson, University of Arizona Press, p. 931–968.

Suppe, J., and Connors, C., 1992, Critical taper wedge mechanics of fold-thrust-belts on Venus: Initial result from *Magellan*: Journal of Geophysical Research, v. 97, p. 13 545–13 562.

Tanaka, K.L., Moore, H.J., Schaber, G.G., Chapman, M.G., Stofan, E.R., Campbell, D.B., Davis, P.A., Guest, J.E., McGill, G.E., Rogers, P.G., Saunders, R.S., and Zimbelman, J.R., 1994, The Venus geologic mappers' handbook (second edition): U.S. Geological Survey Open-File Report OFR-94–438, 50 p.

Withjack, M.O., and Scheiner, C., 1982, Fault patterns associated with domes—An experimental and analytical study: American Association of Petroleum Geologists Bulletin, v. 66, p. 302–316.

Young, D.A., Hansen, V.L., and Bleamaster, L.F., 2000, The plains of Aphrodite: Styles and history of volcanic resurfacing: Eos (Transactions, American Geophysical Union), v. 81, no. 48, p. F700, abstract P52A-05.

MANUSCRIPT RECEIVED BY THE SOCIETY MARCH 26, 2001
REVISED MANUSCRIPT RECEIVED FEBRUARY 8, 2002
MANUSCRIPT ACCEPTED FEBRUARY 25, 2002

Printed in the USA